

ABIOTIC FORMATION OF CARBOXYLIC ACIDS (RCOOH) IN INTERSTELLAR AND SOLAR SYSTEM MODEL ICES

Y. S. KIM¹ AND R. I. KAISER^{1,2}

¹ Department of Chemistry, University of Hawaii at Manoa, Honolulu, HI 96822, USA; ralfk@hawaii.edu

² NASA Astrobiology Institute, University of Hawaii at Manoa, Honolulu, HI 96822, USA

Received 2010 August 15; accepted 2010 September 20; published 2010 November 22

ABSTRACT

The present laboratory study simulated the abiotic formation of carboxylic acids (RCOOH) in interstellar and solar system model ices of carbon dioxide (CO₂)–hydrocarbon mix C_nH_{2n+2} ($n = 1$ –6). The pristine model ices were irradiated at 10 K under contamination-free, ultrahigh vacuum conditions with energetic electrons generated in the track of galactic cosmic-ray particles. The chemical processing of the ices was monitored by a Fourier transform infrared spectrometer and a quadrupole mass spectrometer during the irradiation phase and subsequent warm-up phases on line and in situ in order to extract qualitative (carriers) and quantitative (rate constants and yields) information on the newly synthesized species. Carboxylic acids were identified to be the main carrier, together with carbon monoxide (CO) and a trace of formyl (HCO) and hydroxycarbonyl (HOCO) radicals at 10 K. The upper limit of acid column density at 10 K was estimated as much as $(1.2 \pm 0.1) \times 10^{17}$ molecules cm⁻² at doses of 17 ± 2 eV molecule⁻¹, or the yield of $39\% \pm 4\%$ from the initial column density of carbon dioxide. The temporal column density profiles of the products were then numerically fit using two independent kinetic schemes of reaction mechanisms. Finally, we transfer this laboratory simulation to star-forming regions of the interstellar medium, wherein cosmic-ray-induced processing of icy grains at temperatures as low as 10 K could contribute to the current level of chemical complexity as evidenced in astronomical observations and in extracts of carbonaceous meteorites.

Key words: astrobiology – astrochemistry – cosmic rays – ISM: molecules – methods: laboratory – planets and satellites: general

Online-only material: color figures

1. INTRODUCTION

Complex organic molecules act as molecular tracers to understand the astrochemical evolution of the interstellar medium (ISM). Carboxylic acids (RCOOH)—organic molecules which carry the COOH group—have received special attention during the last years due to their crucial role in astrobiology (Pizzarello 2007) since they are considered as important biomarkers and intermediates to amino acids and proteins (Schidlowski 1993). To date, two carboxylic acids have been detected in the gas phase of the ISM. Acetic acid (CH₃COOH) was monitored toward star-forming regions such as Sgr B2, being the second to interstellar formic acid (HCOOH) in the family of carboxylic acids (Mehring et al. 1997; Remijan et al. 2002, 2003; Cazaux et al. 2003; Shiao et al. 2010). Among the hot core sources, Sgr B2 (N-LMH) is the primary target of observational and theoretical interests in that it is the only source where three C₂H₄O₂ isomers, acetic acid (CH₃COOH), methyl formate (HCOOCH₃), and glycoaldehyde (HCOCH₂OH) were identified (Hollis et al. 2001; Remijan et al. 2003; Lattelais et al. 2009; Puletti et al. 2010). Hollis et al. (2001) estimated the relative abundances of 1 (CH₃COOH):26 (HCOOCH₃):0.5 (HCOCH₂OH). However, despite the recognized presence of carboxylic acids in hot molecular cores, their formation routes are still debatable. Ehrenfreund & Charnley (2000) proposed ion–molecule routes involving the protonation of mantle-formed molecules such as methanol (CH₃OH) followed by a reaction with formic acid in the gas phase and a postulated dissociative recombination leading to acetic acid (Ehrenfreund et al. 2001):



In the following years, however, these ion–molecule schemes were challenged by grain surface proponents, who asserted that those steps such as reactions (1) and (2) would be energetically unfavorable relative to competing channels including multiple-body fragmentations (Garrod & Herbst 2006; Garrod et al. 2008). Nonetheless, Shiao et al. (2010) postulated the critical roles of both gas phase and grain surface reactions to form acetic acid in the ISM.

The presence of extraterrestrial carboxylic acids is not only restricted to the gas phase. Those carboxylic acids bearing straight/branched carbon chains up to eight carbon atoms were also sampled in extracts of the Murchison meteorite, a carbonaceous chondrite (Yuen & Kvenvolden 1973; Cronin & Chang 1993; Botta & Bada 2002). In particular, the distribution of straight-chain acids was reported fit in general molecular formula of C_nH_{2n+1}COOH ($n = 1$ –7), i.e., with increasing chain length acetic acid, propanoic acid, butanoic acid, pentanoic acid, hexanoic acid, heptanoic acid, and octanoic acid. The recent advances on extraction methods further benefited Huang et al. (2005) to recover even a larger suite of carboxylic acids in Murchison: as much as 50 aliphatic acids enriched in stable isotopes beyond terrestrial levels of contamination were detected. In this process, the indigenous nature of formic acid (HCOOH) was not only confirmed by its deuterium (D) enrichment, but a systematic trend in Murchison was also drawn in the dominance of branched-chain acids with multiple methyl (CH₃) and ethyl (C₂H₅) groups over straight-chain counterparts. Martins et al. (2006) managed to recover “free” dicarboxylic acids in Murchison under a mild condition, wherein butanedioic acid (C₂H₄(COOH)₂) and methyl butanedioic acid were extracted to be the most abundant, providing an organic record of the parent body processing in extraterrestrial origin. In the context of organics in our solar system, it is important to note that the

sustainability of carboxylic acids has yet to be demonstrated under carbon-dioxide-rich planetary surface environments such as in Mars (Benner et al. 2000; Stalport et al. 2009) and in Saturn's icy satellites (Filacchione et al. 2010). For instance, the Viking's in situ gas chromatography–mass spectrometry (GC–MS) analysis on Martian landing sites did not prove the presence of any organic acids such as acetic acid (CH_3COOH), oxalic acid $(\text{COOH})_2$, or mellitic acid ($\text{C}_6(\text{COOH})_6$) (Benner et al. 2000). The lacking evidence was attributable to processes acting on the Martian surface that may have degraded the organic acids either back to volatile gases or transformed the acids to non-volatile acid derivatives such as their salts and anhydrides (Stalport et al. 2009; Hintze et al. 2010; Dartnell et al. 2007; Bernstein et al. 2004).

In spite of the growing number/interests of indigenous discovery, there have been only few laboratory simulations to address the abiotic formation of carboxylic acids in interstellar and cometary ice analogs. McDonald et al. (1996) conducted plasma discharge irradiation of water (H_2O)/methanol (CH_3OH)/carbon dioxide (CO_2)/ethane (C_2H_6) ices condensed at liquid nitrogen (77 K) temperature. The reaction products were then recovered by methanol extraction and analyzed by spectroscopic and chromatographic techniques. Polyalcohol functionality was evident together with carbonyl-containing groups of ketones and esters. The presence of acetic acid (CH_3COOH) was firmly established, while formic (HCOOH) and glycolic (HOCH_2COOH) acids were proposed at tentative levels. Muñoz Caro & Schutte (2003) also reported the formation of carboxylic acid salts in photo-processed interstellar ice analogs. In contrast, Kaiser et al. (1995a) prepared methane (CH_4) and molecular O_2 (1%–2%) ices under the ultrahigh vacuum (UHV) conditions and irradiated the ice samples with 9 MeV α particles up to doses of 30 eV molecule⁻¹. The irradiated ices at either at 10 K or 50 K were then warmed up to 293 K and subsequently subject to GC–MS analyses for the carboxylic acid detection. A suite of primary acids were reported in range of $\text{C}_{13}\text{H}_{27}\text{COOH}$ – $\text{C}_{19}\text{H}_{29}\text{COOH}$ along with some unidentified alcohols. In subsequent studies, Zheng & Kaiser (2007) utilized energetic electrons to mimic the processing of secondary electrons formed in the track of galactic cosmic-ray (GCR) particles. Accordingly, water (H_2O) and carbon dioxide (CO_2) ices were targeted at 10, 40, and 60 K; carbonic acid (H_2CO_3) was identified to be the main product in irradiated ices with radiation doses reaching 5–8 eV molecule⁻¹. Traces of formic acid (HCOOH) or formaldehyde (H_2CO) were deemed to be present. Based on their reaction mechanisms and kinetic studies, the following sequential reactions (3–5) were proposed. It begins with the radiolysis-induced cleavage of O–H bond of a water molecule in a pre-complex with carbon dioxide, providing the atomic hydrogen (H) with excess kinetic energies available for the subsequent reaction with a neighboring carbon dioxide molecule forming the *trans*-HOCO radical (4). As two nascent neighboring radicals HOCO and OH recombine within the matrix cage and form carbonic acid (5):

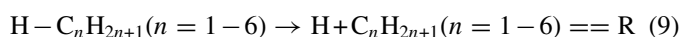


In the same year, Bennett & Kaiser (2007) simulated the radiation-induced formation of acetic acid (CH_3COOH) in methane (CH_4) and carbon dioxide (CO_2) ices via the key

intermediate, *trans*-HOCO. In a reaction sequence (6–8) similar to (3–5), acetic acid was formed via a consecutive reaction sequence (6–8):



The kinetics studies on the CH_4/CO_2 and $\text{H}_2\text{O}/\text{CO}_2$ systems suggest that any hydrocarbon ($\text{C}_n\text{H}_{2n+2}$) and hydride might undergo radiation-induced unimolecular decomposition to atomic hydrogen and a hydrocarbon radical. Hydrogen could react with carbon dioxide to the *trans*-HOCO radical, which recombines in the matrix cage with the hydrocarbon radical for a carboxylic acid (reactions 9–11)). The primary goal of this study is to test this hypothesis and to investigate to what extent carbon dioxide–hydrocarbon mix, $\text{C}_n\text{H}_{2n+2}$ ($n = 1$ –6), will form a mixture of carboxylic acids at 10 K in interstellar and solar system model ices. This will also lead to the understanding of the detection of the wide range of carboxylic acids that possibly mimic the distribution of those found in Murchison:



2. EXPERIMENTAL DETAILS

The experiments were conducted in a UHV chamber with the base pressure in the low 10^{-11} torr range (Bennett et al. 2004). Contamination-free vacuum conditions were rendered by a magnetically suspended turbo pump (1100 l s⁻¹) backed by an oil-free scroll pump. A differentially pumped rotary platform, which holds a highly polished silver mirror as a substrate for the ice condensation, is positioned in the center of the chamber. Interfaced with the platform are a two-stage closed-cycle helium refrigerator and a feedthrough for the programmable temperature controller. The temperature of the silver crystal can be regulated with a precision of ± 0.3 K between 10 and 330 K. The gas mixture was prepared in a gas mixing chamber by the sequential addition of 1 mbar of carbon dioxide (CO_2 ; 99.999%; BOC Gases) and 500 mbar of hydrocarbon mix in helium ($\text{C}_n\text{H}_{2n+2}$, $n = 1$ –6; 1000 ppm each; Matheson). The premixed gases were then deposited to the silver target at 10 K via a precision leak valve and a glass capillary array positioned 5 mm in front of the silver substrate. The deposition was carried out for 60 minutes at an inlet pressure of 4.0×10^{-7} torr. The mid-infrared spectra of solid samples were recorded from 6000 to 400 cm⁻¹ with 4 cm⁻¹ spectral resolution utilizing a Nicolet 6700 FTIR unit. The gas phase was monitored by a quadrupole mass spectrometer (Balzer QMG 420) operating in a residual gas analyzer mode with electron impact ionization energy of 100 eV and a mass range of up to 200 amu.

Figure 1(a) depicts a mid-infrared spectrum of the ice mixture as deposited at 10 K. The vibrational assignments are compared with literature values in Table 1 (Bennett et al. 2004; Moore & Hudson 2003; Socrates 2001). As demonstrated earlier in the binary system of carbon dioxide (CO_2) and methane (CH_4) ices (Bennett & Kaiser 2007), our deposition conditions lead to a composite ice film, the infrared spectrum of which matches that of each individual component (Table 1). The column density

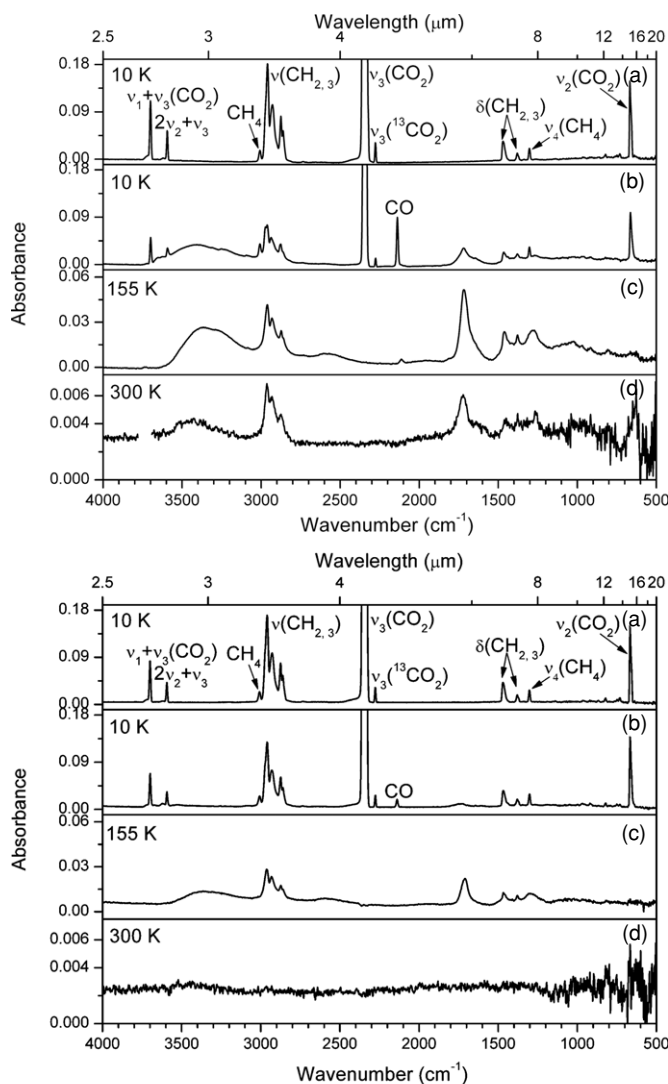


Figure 1. Mid-infrared spectra of carbon dioxide (CO₂) and hydrocarbon (C_nH_{2n+2}; *n* = 1–6) ices recorded before (a) and after (b) irradiation with 1 μA (top) and 0.1 μA (bottom) at 10 K. Also shown are the corresponding spectra at 155 K (c) and at 300 K (d) recorded in the subsequent warm-up phases, once after volatile products have sublimed off the substrate along with the initial ice mixture. For (d) with 1 μA, the high-frequency contribution of atmospheric water and carbon dioxide was traced out of the residue spectrum. The absorption features ranging 1900–1100 cm⁻¹ are deconvoluted and detailed in Figure 2. The individual band assignments are compiled in Table 1.

(molecules cm⁻²) of carbon dioxide was estimated utilizing an integrated absorption coefficient of 1.4×10^{-18} cm molecule⁻¹ for the $\nu_1 + \nu_3$ at 3700 cm⁻¹ (Bennett et al. 2004) to be $(3.0 \pm 0.2) \times 10^{17}$ molecules cm⁻²; this translates into an ice thickness of 128 ± 10 nm after taking into account a solid density of 1.7 g cm⁻³. The methane component was directly evaluated via ν_4 at 1300 cm⁻¹, yielding the column density of $(1.9 \pm 0.2) \times 10^{16}$ molecules cm⁻² and the ice thickness of 9.5 ± 1.0 nm utilizing an absorption coefficient of 4.0×10^{-17} cm molecule⁻¹ (Bohn et al. 1994) and a density of 0.517 g cm⁻³ (Donnay & Ondik 1972). Concerning the component of the higher hydrocarbons (C_nH_{2n+2}; *n* = 2–6), the band at 1460 cm⁻¹ was chosen to represent those group transitions (Table 1). Accordingly, the absorption coefficient of this band was determined to be 3.1×10^{-18} cm molecule⁻¹, resulting in the column density and the ice thickness of the five hydrocarbon components

to be $(7.5 \pm 0.8) \times 10^{16}$ molecules cm⁻² and 80 ± 9 nm, respectively (Refson & Pawley 1986). However, it is important to investigate the relative fraction of C1–C6 hydrocarbons in the ice mixture. This was conducted via a mass spectrometer. First, the ion current profiles of the parent six hydrocarbons, i.e., *m/z* = 16 (CH₄), 30 (C₂H₆), 44 (C₃H₈), 58 (C₄H₁₀), 72 (C₅H₁₂), and 86 (C₆H₁₄) in the mixture of a well-defined composition of 1:1:1:1:1:1, were introduced into the chamber at room temperature without condensing the hydrocarbons. For comparison, the condensed ices were sublimed by heating the target to 300 K with a gradient of 0.5 K minute⁻¹. The relative, integrated areas of the ion currents were then compared to the recorded ion currents of the calibration gas mixture (Zheng et al. 2006, 2008). This leads to a relative abundance in the solid ices of (1.3:0.9:1.0:0.9:1.0:1.0) ± 0.1 from methane to hexane within 1σ error level. The use of a calibration standard of known composition avoids correction factors for the differences in ionization efficiencies and pumping speeds (Kaiser et al. 1995b).

The ices were then irradiated isothermally for 60 minutes with 5 keV electrons at a nominal beam current of 0 (blank), 100 nA, and 1 μA. The electron beams were generated with an electron gun (Specs EQ 22–35) and scanned over the target area of 3.2 ± 0.3 cm² to avoid heating of the target. Note that actual extraction efficiency of the electron gun is stated to be 78.8%, thus correcting the fluence down to 5.5×10^{15} electrons cm⁻² hitting the target at a nominal current of 1 μA over 60 minutes. The electron trajectories and energy loss in layers of the ice system were simulated using the CASINO code (Drouin et al. 2001). These calculations yield an averaged transmitted energy of the electrons at about 3.80 keV; this indicates that 1.2 keV per impinging electron were transferred to the ices. This value corresponds to an average linear energy transfer (LET) of 5.5 keV μm⁻¹, the order of magnitudes that 10–20 MeV cosmic rays typically transfer to interstellar ices, i.e., a few keV μm⁻¹ (Kaiser & Roessler 1997). Therefore, the deposited ices receive an average dose of up to 17 ± 2 eV molecule⁻¹ during the 1 hr exposure at 1 μA. After the irradiation, the ices are kept isothermally for 60 minutes before being heated to 300 K with a gradient of 0.5 K minute⁻¹. This allows the sublimed molecules to be detected by the quadrupole mass spectrometer.

3. RESULTS

3.1. Infrared Spectroscopy

First, we will investigate the radiation-induced formation of new species in carbon dioxide (CO₂)–hydrocarbon (C_nH_{2n+2}; *n* = 1–6) ices. Figure 1 displays the infrared spectra of ices recorded at 10 K before (a) and after (b) the irradiation with 1 μA (top) and 0.1 μA (bottom). Also shown are the corresponding spectra at 155 K (c) and at 300 K (d) recorded in the subsequent warm-up phases, once volatile reactants sublimed off the substrate. The atmospheric water and carbon dioxide interferences were traced out of the high-frequency side of (d) spectrum with 1 μA.

The radiation exposure at 10 K leads to multiple new absorption features. A list of carriers, by virtue of clarity, is defined by the functional groups rather than individual molecules and compiled along with the vibrational assignments in Table 1. Carboxylic acids (RCOOH) were identified to be the main carrier, together with carbon monoxide (CO) at 2139 cm⁻¹ and a trace of formyl (HCO) and hydroxycarbonyl (HOCO) radicals at about 1852 cm⁻¹ (Bennett & Kaiser 2007). Note that abundances of HOCO radical in current matrices remained in

Table 1
Infrared Absorption Features Recorded Before and After Irradiation of Carbon Dioxide (CO₂) and Hydrocarbon (C_nH_{2n+2}; n = 1–6) Ices at 10 K and During Warm-up Phases at 155 and 300 K.

Before Irradiation 10 K (cm ⁻¹)	After Irradiation ^a 10 K (cm ⁻¹)	Warm-up ^a		Literature Assignment	
		155 K (cm ⁻¹)	300 K (cm ⁻¹)	(cm ⁻¹)	Carrier
3700	3708 ^b	$\nu_1+\nu_3(\text{CO}_2)$
3594	3600 ^b	$2\nu_2+\nu_3(\text{CO}_2)$
...	3525 ^c	3580–3500 ^d	$\nu(\text{OH, acid monomers})$
...	3600–2500	3431, 3267	3430, 3226	3300–2500 ^d	$\nu(\text{OH, carboxylic acids})$
		2922, 2745	2952	3300 ^e	$\nu(\text{OH, alcohols})$
		2590			
...	...	3086	...	3150–3000 ^d	=CH ₂ asym stretch
3008	3011 ^f	$\nu_3(\text{CH}_4)$
2960	...	2964	2966	2975–2950 ^d	–CH ₃ asym stretch
2929	...	2929	2929	2940–2915 ^d	–CH ₂ – asym stretch
2875	...	2869	2873	2885–2865 ^d	–CH ₃ sym stretch
2861	–CH ₂ – sym stretch
2360, 2332	2342 ^b	$\nu_3(\text{CO}_2)$
2277	2282 ^b	$\nu_3(^{13}\text{CO}_2)$
...	2139	2139 ^b	$\nu(\text{CO})$
...	1852 ^g	1853 ^h	$\nu(\text{C=O, HCO radical})$
				1847 ^h , 1839 ^h	$\nu(\text{C=O, HOCO radical})$
...	1740 ^c , 1720	1718	1724	1740–1700 ^d	$\nu(\text{C=O, carboxylic acids})$
...	1719	1720–1697 ⁱ	$\nu(\text{C=O, R(H)}_2\text{CO})$
...	1642	1680–1620 ^d	$\nu(\text{C=C, alkenes})$
...	1640	1689	1630	1660 ^e	$\nu(\text{C=O/C=C})$
					$\nu(\text{C=O with } \beta \text{ OH group})$
1466	...	1461	1449	1465–1440 ^d	–CH ₃ asym deform
					–CH ₂ – scissor
...	1439	1439	...	1440–1360 ^d	=CH ₂ scissor
...	1384	1421	1316	1440–1395 ^d	$\delta(\text{C–O–H, acid dimers})$
				1380–1280 ^d	$\delta(\text{C–O–H, acid monomers})$
1379	...	1377	1378	1390–1370 ^d	–CH ₃ sym deform
1303	1298 ^f	$\nu_4(\text{CH}_4)$
...	1269, 1212	1282	1262	1320–1210 ^d	$\nu(\text{C–O, carboxylic acids})$
...	...	1081, 1023	1024, 948	1090–1000 ^d	$\nu(\text{C–OH, primary alcohols})$
				970–875 ^d	$\tau(\text{O–H, carboxylic acids})$
664	655 ^b	$\nu_2(\text{CO}_2)$
...	...	649	639	649 ^j	$\delta(\text{O–C=O, carboxylic acids})$

Notes. 60 minutes irradiation (0.1 μA , 1 μA) on ices with 5 keV electrons.

^a Only new absorption features reported in irradiated ices at 10 K; only heavier radiation products remained on the substrate at 155 K, after lighter products sublimed at lower temperatures along with the initial ice mixture.

^b Bennett et al. (2004).

^c Only with 0.1 μA current.

^d Socrates (2001).

^e McDonald et al. (1996).

^f Moore & Hudson (2003).

^g Double hump feature in the baseline ranging 1857–1830 cm^{-1} .

^h Bennett & Kaiser (2007).

ⁱ DelloRusso et al. (1993).

^j Sander & Gantenberg (2005).

trace levels. Components of ketones/aldehydes (R(H)₂CO) and alkenes were also recognizable at the end of irradiation at 10 K. In particular, carboxylic acids were evidenced in irradiated ices at 10 K by the characteristics of carbonyl $\nu(\text{C}=\text{O})$ and hydroxyl $\nu(\text{OH})$ at about 1740–1720 and 3600–2500 cm^{-1} , respectively (Table 1; Socrates 2001). The presence of alcohols (ROH) was probable but inconclusive at 10 K in that the broad absorption features in range of 3600–2500 cm^{-1} would cover up the hydroxyl $\nu(\text{OH})$ of alcohol at 3300 cm^{-1} and that the flat baseline in range of 1100–1000 cm^{-1} would be insufficient for assigning to $\nu(\text{C–O})/\nu(\text{C–C})$, the other characteristic of alcohols reported in McDonald et al. (1996; Table 1). Two additional bands of carboxylic acids were further evi-

denced in the lower frequency regions, $\nu(\text{C–O})$ in a doublet of 1269 and 1212 cm^{-1} , and $\delta(\text{C–O–H})$ in a broad absorption centering at 1384 cm^{-1} (Table 1). This identification is in accord with Sander & Gantenberg (2005), who investigated the dimerization/aggregation of acetic acid (CH₃CO₂H) and propanoic acid (C₂H₅CO₂H) in argon matrices. Monomeric $\nu(\text{C}=\text{O})$ was reported in matrices at about 1780 cm^{-1} and redshifted by 60 cm^{-1} upon aggregation, while the corresponding $\nu(\text{O–H})$ at about 3570 cm^{-1} transformed into a symmetric multi-band pattern ranging 3200–2500 cm^{-1} upon aggregation.

Figure 1(c) depicts the spectrum recorded during warm-up phases at 155 K offering a snapshot of heavier radiation products after the rest of volatile solids have sublimed at lower

Table 2
Production Yield in Irradiated Carbon Dioxide (CO₂) and Hydrocarbon (C_nH_{2n+2}; n = 1–6) Ices at 10 K and Corresponding Change During Warm-up Phases at 155 and 300 K.

Current (μA)	Temperature (K)	CO (molecules cm ⁻²)	RCO ₂ H ^a (molecules cm ⁻²)	ΔCO ₂ ^b (molecules cm ⁻²)
0.1	10	(0.7 ± 0.0) × 10 ¹⁶	(6.7 ± 0.6) × 10 ¹⁶	-8.3 × 10 ¹⁶
1	10	(3.5 ± 0.2) × 10 ¹⁶	(11.5 ± 1.2) × 10 ¹⁶	-18.8 × 10 ¹⁶
Warm-up phases after 1 μA at 10 K				
...	155	...	(9.1 ± 0.8) × 10 ¹⁶	...
...	300	...	(1.1 ± 0.1) × 10 ¹⁶	...

Notes. 60 minutes irradiation of ices with 5 keV electrons. Ice values with 0.1 μA factored by 1.43.

^a Upper limit derived as described in Section 3.1.

^b Amount destroyed from the initial [CO₂]₀ = (3.0 ± 0.2) × 10¹⁷ molecules cm⁻².

temperatures off the substrate–hexane (C₆H₁₄), the heaviest condensed reactant, sublimates peaking at about 140 K. By this stage, carboxylic acids (RCO₂H) turn in a multiple-structured ν(O–H) stretching 3500–2500 cm⁻¹, an intensified ν(C = O) at about 1720 cm⁻¹, as well as a singlet ν(C–O) at 1282 cm⁻¹. A concrete assignment of carboxylic acids was possible as compiled in Table 1. The alkyl functionality of carboxylic acids was further corroborated in those CH₃/CH₂ group stretches at 2964, 2929, and 2869 cm⁻¹, as well as in those deformations at 1461 and 1377 cm⁻¹. Residual alkenes were recognized at 3086, 1689, and 1439 cm⁻¹ in good agreements with literature assignments (Kim et al. 2010; Socrates 2001; McDonald et al. 1996) (Table 1). More probable at this stage were the alcohol (ROH) absorptions at 3300 and 1050 cm⁻¹ regions, as if they were blended in stronger absorptions of carboxylic acids (RCO₂H) (Bennett et al. 2007). A successive heating to room temperature even resulted in the sublimation of those carriers to the residual level under the UHV conditions (Figure 1(d)). Nonetheless, these are characteristics of carboxylic acids still persistent in the residue spectrum: ν(O–H) notably with the high-frequency portion, ν(C = O) at about 1720 cm⁻¹, ν(C–O) at 1262 cm⁻¹, and δ(O–C = O) at 639 cm⁻¹ (Table 1).

Second, we attempted to quantify the production yield of carboxylic acids (RCO₂H) in irradiated ices. Figure 2 depicts the infrared spectra ranging 1900–1100 cm⁻¹ that exemplify temporal changes of products and reactants during 1 μA irradiation at 10 K (bottom) and the subsequent warm-up phases at 155 K (middle) reaching 300 K (top). All spectra traces in this figure were deconvoluted into contributing components of Gaussians, making possible the temporal quantification of carboxylic acids during radiation exposure at 10 K. The same methodology was applied to the irradiation ices with 0.1 μA (Table 2). The carbonyl stretch ν(C = O) of carboxylic acids at 1720 cm⁻¹ was unambiguously distinguished from the adjacent others, particularly from the component at 1640 cm⁻¹, which is attributable to the group ν(C = O/C = C) (McDonald et al. 1996). Two minor components of 1719 and 1642 cm⁻¹ were only present at 10 K, then vanishing off at the higher temperatures (Figure 2). The former was attributable to ν(C = O) of R(H)₂CO (DelloRusso et al. 1993) and the latter to ν(C = C) of alkenes (Table 1). Temporal changes (molecules cm⁻²) of carboxylic acids, [RCOOH]_t, were accordingly derived in reaction (12) during radiation exposure at 10 K, where A₁₇₂₀ and A₁₆₄₀ correspond to those integrated Gaussians at 1720 and 1640 cm⁻¹ given a temporal spectrum, respectively (Figure 2). The production of carbon monoxide (CO) in [CO]_t was monitored by evaluating the fundamental at 2139 cm⁻¹

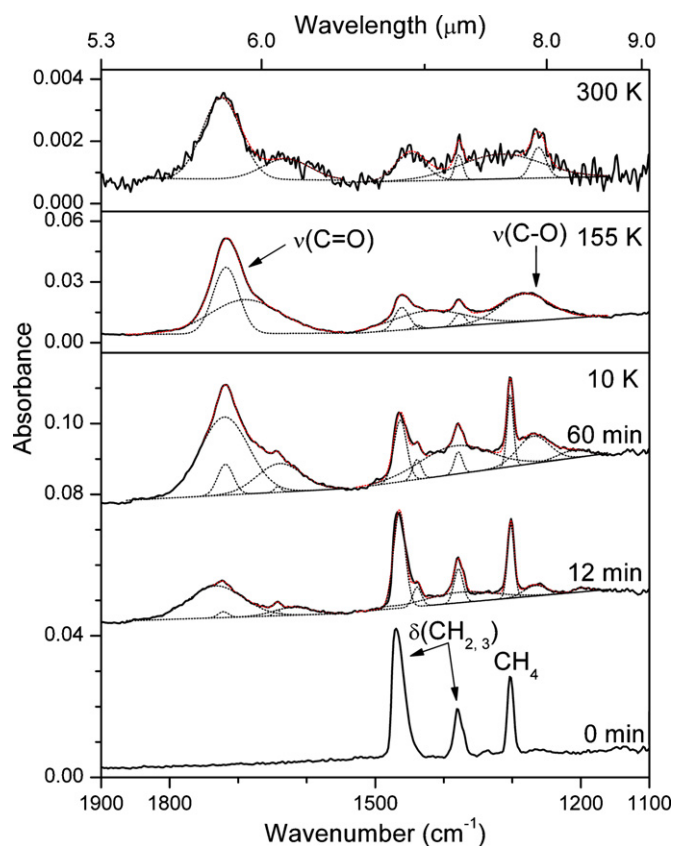


Figure 2. Infrared spectra in the range of 1900–1100 cm⁻¹ (5–9 μm) monitoring temporal changes of products and reactants during 1 μA irradiation at 10 K (bottom) and the subsequent warm-up phases at 155 K (middle) reaching 300 K (top). Carboxylic acids (RCOOH) were assigned the main carrier of ν(C=O) and ν(C–O) at about 1720 and 1250 cm⁻¹, respectively, at all temperatures. The absorption features are accordingly deconvoluted with Gaussians and assigned in Table 1. The set of Gaussians (black-dotted line) are shown on a linear baseline along with the resulting fit (red-dotted line) overlaid in spectrum. (A color version of this figure is available in the online journal.)

along with the reported A value of 1.1×10^{-17} cm molecule⁻¹ (Jamieson et al. 2006). The marginal *trans*-HOCO production in [COOH]_t was recognized at about 1850 cm⁻¹ (Table 1):

$$[\text{RCOOH}]_t \leq \frac{A_{1720}}{A_{1720} + A_{1640}} ([\text{CO}_2]_0 - [\text{CO}_2]_t - [\text{CO}]_t + [\text{COOH}]_t) \quad (12)$$

In this way, the upper limit of acid column density was derived

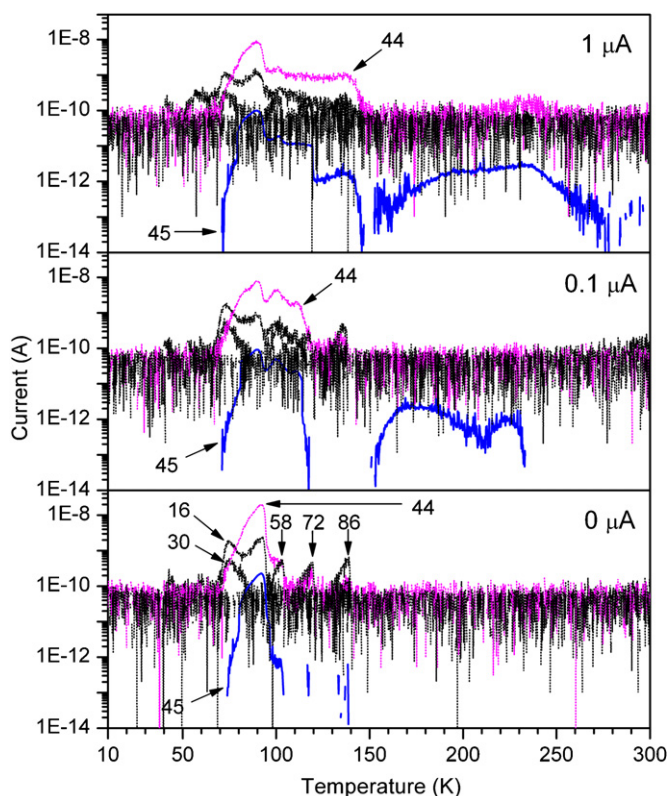


Figure 3. Temporal evolution of the ion currents associated with molecular carbon dioxide (CO_2 ; $m/z = 44$), and six hydrocarbons ($\text{C}_n\text{H}_{2n+2}$; $n = 1-6$; $m/z = 16, 30, 44, 58, 72, 86$) released during warm-up phases after $0 \mu\text{A}$ (bottom), $0.1 \mu\text{A}$ (middle) and $1 \mu\text{A}$ (top) irradiation of the ice mixture at 10 K. Note that the ion current of $m/z = 45$ serves to trace a natural abundance of carbon dioxide ($^{13}\text{CO}_2$) released below 150 K and a mass fragment (COOH^+) of carboxylic acids (RCOOH) released at higher temperatures. Traces are color-coded for clarity.

(A color version of this figure is available in the online journal.)

at $(1.2 \pm 0.1) \times 10^{17}$ molecules cm^{-2} by the end of $1 \mu\text{A}$ irradiation, or the yield of $39\% \pm 4\%$ given the initial column density of $[\text{CO}_2]_0 = (3.0 \pm 0.2) \times 10^{17}$ molecules cm^{-2} (Table 2). With the reference in irradiated ices at 10 K, carboxylic acid column densities during warm-up phases were compared down to $(9.1 \pm 0.8) \times 10^{16}$ molecules cm^{-2} at 155 K and further down to $(1.1 \pm 0.1) \times 10^{16}$ molecules cm^{-2} at 300 K (Figure 2). With a current of $0.1 \mu\text{A}$, the formation of carboxylic acids at 10 K slowed down at $(6.7 \pm 0.6) \times 10^{16}$ molecules cm^{-2} after a normalization, as was the yield down at $22\% \pm 3\%$ (Table 2).

3.2. Mass Spectrometry

It is of interest to correlate the infrared observation with a mass spectroscopic analysis of the gas phase. Figure 3 displays temporal evolution of the ion currents associated with carbon dioxide (CO_2 ; $m/z = 44$), and six hydrocarbons ($\text{C}_n\text{H}_{2n+2}$; $n = 1-6$; $m/z = 16, 30, 44, 58, 72, 86$) released during warm-up phases after $0 \mu\text{A}$ (bottom), $0.1 \mu\text{A}$ (middle), and $1 \mu\text{A}$ (top) irradiation of the ice mixture at 10 K. It is worthwhile to stress that none of the newly formed species was detected in the residual gas analyzer during actual irradiation phase, but only detected in the sublimation phases of the irradiated ices. Molecular ion currents of RCOOH ($\text{C}_n\text{H}_{2n+1}\text{COOH}$; $n = 1-6$; $m/z = 60, 74, 88, 102, 116, 130$) were not detected due to the high setting (100 eV) of electron impact ionization energy.

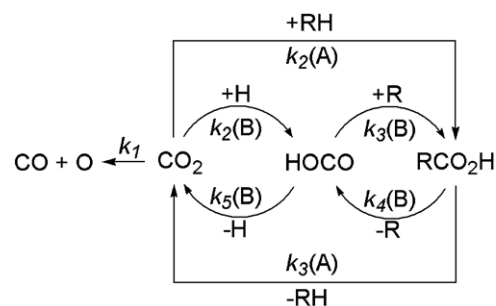


Figure 4. Reaction schemes (pathways A and B) used to fit temporal profiles of the species produced during radiation exposure ($0.1 \mu\text{A}$, $1 \mu\text{A}$) of carbon dioxide and hydrocarbon ices at 10 K.

Instead, ion current of $m/z = 45$ served to trace a natural abundance of carbon dioxide ($^{13}\text{CO}_2$) released below 150 K and to trace a mass fragment (COOH^+) of those carboxylic acids (RCOOH) released at higher temperatures, as shown in the middle and top panels of Figure 3. As correlated with infrared spectroscopy in Section 3.1, the lower emission ($0.1 \mu\text{A}$) caused this ion current to level off below 250 K, while the higher emission ($1 \mu\text{A}$) far up to 300 K. As the ion current of $m/z = 45$ increased in the gas phase, the infrared absorptions decreased in the solid state.

4. DISCUSSION

4.1. Reaction Mechanisms

Having assigned the carriers of the newly formed species (Table 1) and quantified the production yield in irradiated carbon dioxide (CO_2)–hydrocarbon ($\text{C}_n\text{H}_{2n+2}$; $n = 1-6$) ices (Table 2), we are attempting now to elucidate the underlying reaction mechanisms how carboxylic acids (RCOOH) are synthesized during radiation exposure at 10 K. For this purpose, two sets of kinetic reaction schemes (pathways A and B) were developed (Figure 4) to fit the column densities of species produced during the radiation exposure with $0.1 \mu\text{A}$ and $1 \mu\text{A}$ (Figure 5). A system of four and five coupled differential equations was numerically solved (Frenklach et al. 1992, 2007) for the respective pathways A and B, resulting in the corresponding set of rate constants derived (Table 3).

As described in Section 2, the temporal profile of carbon dioxide (CO_2) was monitored by the decay of combination band at 3700 cm^{-1} ($\nu_1 + \nu_3$). The hour-long radiation exposure to 5 keV electrons at 10 K caused the decrease of CO_2 column density from $(3.0 \pm 0.2) \times 10^{17}$ molecules cm^{-2} to $(2.2 \pm 0.1) \times 10^{17}$ molecules cm^{-2} with $0.1 \mu\text{A}$ and further to $(1.1 \pm 0.2) \times 10^{17}$ molecules cm^{-2} at a current of $1 \mu\text{A}$. Considering the fluence of 5.5×10^{15} electrons cm^{-2} hitting the target, each impinging electron destroys 35 ± 7 carbon dioxide molecules. The following carbon dioxide destruction pathways (reactions 13–16) are considered in this radiolysis of carbon dioxide and hydrocarbon ices:

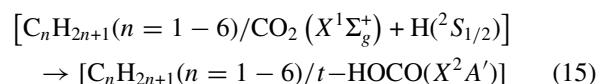
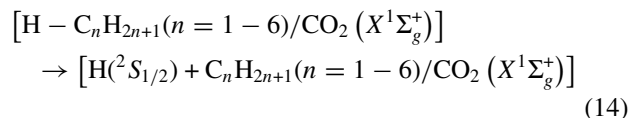
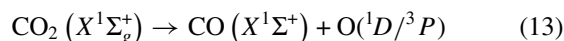


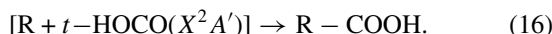
Table 3
Rate Constants Derived Via Iterative Solution to Reaction Schemes in Figure 4.

Reaction		Rate Constant ^a	
		0.1 μA	1 μA
Pathway A			
$\text{CO}_2 \rightarrow \text{CO} + \text{O}$	k_1^a	8.6×10^{-6}	6.5×10^{-5}
$\text{CO}_2 + \text{R-H} \rightarrow \text{RCO}_2\text{H}$	k_2^b	1.1×10^{-4}	7.4×10^{-4}
$\text{RCO}_2\text{H} \rightarrow \text{CO}_2 + \text{R-H}$	k_3^a	2.3×10^{-4}	9.0×10^{-4}
$\text{CO}_2 \rightarrow \text{X}$	k_4^a	1.7×10^{-5}	7.8×10^{-5}
Pathway B			
$\text{CO}_2 \rightarrow \text{CO} + \text{O}$	k_1^a	8.6×10^{-6}	6.6×10^{-5}
$\text{CO}_2 + \text{H} \rightarrow (\text{HOCO})$	k_2^b	1.4×10^{-4}	9.3×10^{-4}
$(\text{R}) + (\text{HOCO}) \rightarrow \text{RCO}_2\text{H}$	k_3^b	$7.2 \times 10^{+1}$	$6.4 \times 10^{+1}$
$\text{RCO}_2\text{H} \rightarrow (\text{R}) + (\text{HOCO})$	k_4^a	$1.5 \times 10^{+1}$	$1.7 \times 10^{+1}$
$(\text{HOCO}) \rightarrow \text{CO}_2 + \text{H}$	k_5^a	1.3×10^{-3}	4.0×10^{-3}

Notes. Column densities of the species in parenthesis only derived numerically. Refer to Section 4.1 for details.

^a Units in s^{-1} (first order).

^b Units in $\text{cm}^2 \text{ molecule}^{-1} \text{ s}^{-1}$ (second order).



Carbon monoxide (CO) is produced in reaction (13) along with an atomic oxygen (O) either in the singlet excited state (1D) or in the triplet ground state (3P) after intersystem crossing. The reaction is indeed endoergic by 532 kJ mol^{-1} (5.51 eV) for the triplet or by 732 kJ mol^{-1} (7.59 eV) for singlet channel (Bennett et al. 2004); the required energies for these endoergic processes are supplied by the energy loss from the energetic electrons (5 keV , $5.5 \times 10^{15} \text{ electrons cm}^{-2}$) passing through the ices with an average LET of $5.5 \text{ keV } \mu\text{m}^{-1}$. It indicates that each electron initiates about six carbon monoxide molecules, translating to 35 eV and 48 eV for the formation of $\text{O}(^3P)/\text{O}(^1D)$ per impinging electron, respectively. The fate of those energetic oxygen atoms is beyond the current coverage. However, these suprathreshold atoms could escape the matrix cage and/or react with neighboring hydrocarbons to the formation of alcohols (ROH; Kaiser et al. 1999). The temporal column densities of carbon monoxide, monitored by the absorption of the fundamental at 2139 cm^{-1} , develop via first-order kinetics in the course of irradiation at 10 K (Figure 5). The two sets of rate constant, k_1 , are found to be invariant to the courses of pathways A and B at the order of $8.6 \times 10^{-6} \text{ s}^{-1}$ with $0.1 \mu\text{A}$ and at about $6.5 \times 10^{-5} \text{ s}^{-1}$ with $1 \mu\text{A}$ (Table 3).

Meanwhile, the reactions (14–16) illustrate the dominant carbon dioxide destruction pathway that leads to the formation of carboxylic acids (RCOOH) with yields of 22% ($0.1 \mu\text{A}$) and 39% ($1 \mu\text{A}$; Table 2). These temporal yields were properly constrained by column density fits derived using two independent reaction schemes (Figure 5). The alkyl radical ($\text{C}_n\text{H}_{2n+1}$) is produced in reaction (14) via cleavage of a carbon–hydrogen bond, which Irlé & Morokuma (2000) computed to be endoergic by either 423 kJ mol^{-1} (4.38 eV) or 415 kJ mol^{-1} (4.30 eV) in an example of *n*-propane (C_3H_8)—providing 8 kJ mol^{-1} preference for the secondary carbon–hydrogen bond cleavage over for the primary one. The hydrogen atoms released in this process could possess as much excess kinetic energy of a few eV as demonstrated in the radiolysis of pure solid methane (CH_4) and ethane (C_2H_6) at 10 K (Bennett et al. 2006; Kim et al. 2010). This kinetic energy might be utilized in overcoming an entrance barrier of 106 kJ mol^{-1}

(1.1 eV) posed in the formation (reaction (15)) of the trans-carboxyl radical (*t*-HOCO; Bennett & Kaiser 2007). Note that *t*-HOCO radical was only detected in traces, and alkyl radical in (reaction (14)) even beyond the detection limit, mutually indicative of a facile radical recombination within the matrix cage to the production of carboxylic acids (RCOOH; reaction (16)) or back reaction to the starting materials (Figure 4). Along the single-step conversion pathway A, carbon dioxide is evidenced to proceed at the forward rate of $k_2 = 1.1 \times 10^{-4} \text{ cm}^2 \text{ molecule}^{-1} \text{ s}^{-1}$ with $0.1 \mu\text{A}$ or of $7.4 \times 10^{-4} \text{ cm}^2 \text{ molecule}^{-1} \text{ s}^{-1}$ with $1 \mu\text{A}$ to RCOOH (Table 3). These rate constants, k_2 , are in turn sensibly recognized in the stepwise pathway B, wherein *t*-HOCO forms at the rate of $k_2 = 1.4 \times 10^{-4} \text{ cm}^2 \text{ molecule}^{-1} \text{ s}^{-1}$ with $0.1 \mu\text{A}$ or $9.3 \times 10^{-4} \text{ cm}^2 \text{ molecule}^{-1} \text{ s}^{-1}$ with $1 \mu\text{A}$, in advance of a facile turnover ($k_3 > 1 \text{ cm}^2 \text{ molecule}^{-1} \text{ s}^{-1}$) to carboxylic acids (RCOOH). As the radiolysis proceeds, back reactions evidently weight in to the retro-formation of CO_2 in both pathways of A and B (Table 3). The last reaction (k_4) worthy of mentioning is the radiolysis-induced formation of unknown species “X” in pathway A only, such as ketones/aldehydes ($\text{R(H)}_2\text{CO}$) or species carrying $\nu(\text{C} = \text{O}/\text{C} = \text{C})$ functional groups, which appeared marginally in matrices, but the formation routes of which were not covered in current studies. To summarize, it should be stressed that we cannot discriminate between model A and B, since both fit the data. However, with respect to the formation for carboxylic acids, both models agree that the formation of carboxylic acids presents a two-step sequence via reactions (R14–R16).

4.2. Carbon Budget

In Section 4.1, we elucidated the underlying reaction mechanisms how carboxylic acids (RCOOH) are synthesized at 10 K during radiation exposure of carbon dioxide (CO_2)–hydrocarbon ($\text{C}_n\text{H}_{2n+2}$; $n = 1\text{--}6$) ices. Note that fractions of heavier reactants ($\text{C}_n\text{H}_{2n+2}$; $n = 3\text{--}6$) were deemed to be responsible for the formation of alkenes (Table 1) and even lighter alkanes ($\text{C}_n\text{H}_{2n+2}$; $n = 1\text{--}2$) during radiation exposure, the latter pair of which in turn sublimed together with the unreacted reactant pair resulting in the apparent disproportion of those ion currents (Figure 3). Briefly in this section, we would like to address the issue of the carbon budget relevant to the synthesis of RCOOH with $1 \mu\text{A}$ experiment. By employing the reaction (12), the upper limit of acid column density was estimated at $(1.2 \pm 0.1) \times 10^{17}$ in irradiated ices at 10 K, equivalent to the yield of $39\% \pm 4\%$ given the initial column density of $[\text{CO}_2]_0 = (3.0 \pm 0.2) \times 10^{17} \text{ molecules cm}^{-2}$. From the side of hydrocarbons ($\text{C}_n\text{H}_{2n+2}$; $n = 1\text{--}6$), however, one could fairly estimate the overproduction of RCOOH in irradiated ices at 10 K, considering that the initial hydrocarbon column densities were combined to be $(9.4 \pm 1.0) \times 10^{16} \text{ molecules cm}^{-2}$ in Section 2. The formation of dicarboxylic acids, oxalic acid (COOH)₂ in particular, could alleviate the apparent excess counting from the hydrocarbon side. Oxalic acid is the simplest dicarboxylic acid likely formed during radiation exposure at 10 K via dimerization (R17) of *t*-HOCO(X^2A'). However, its definite identification remains a challenge. Formed in this way at 10 K, oxalic acid could have survived the UHV conditions imposed on during warm-up phases up to room temperature. Suitable chromatographic analyses in the future will serve to determine whether oxalic acid could be a constituent of the acid residue at 300 K (Table 2):



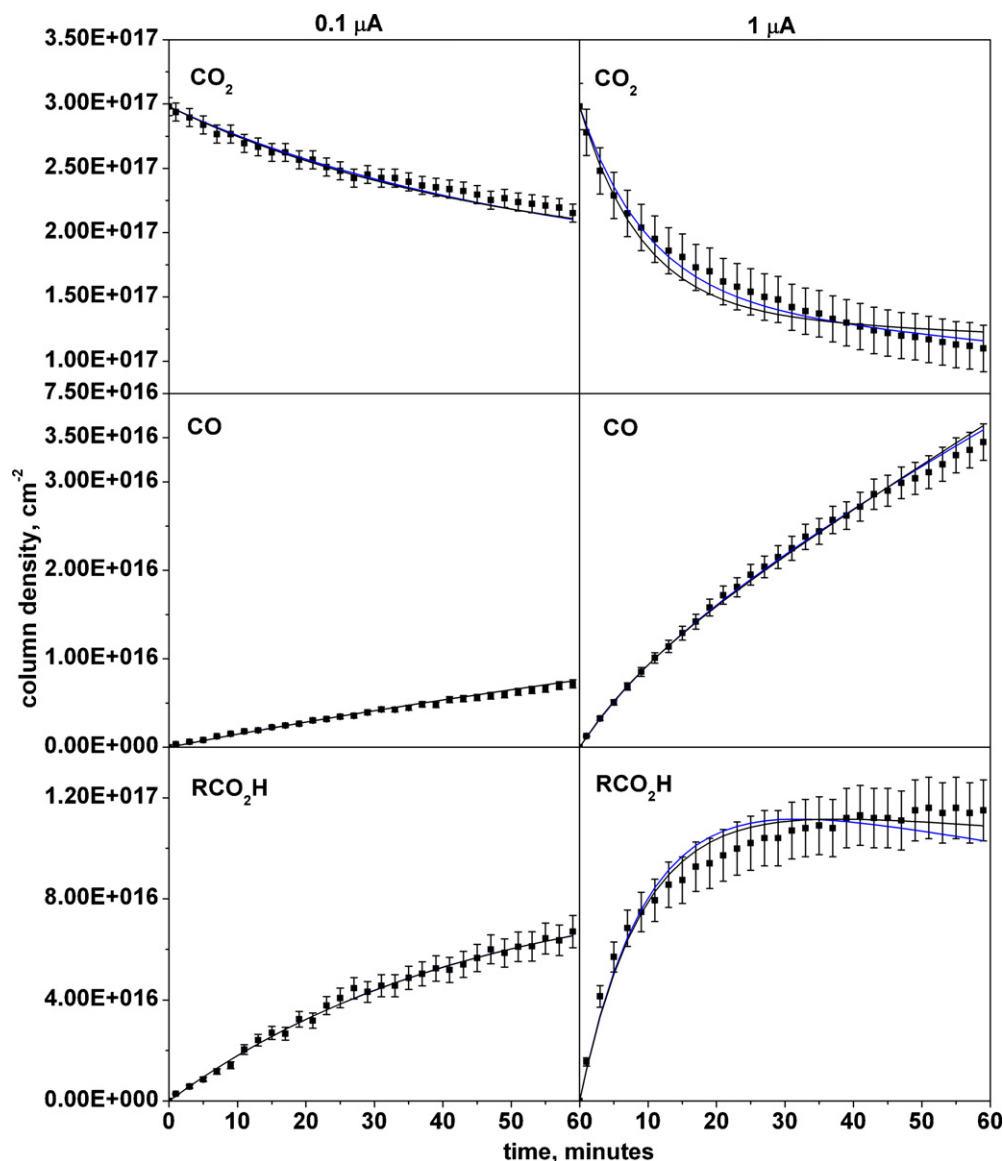


Figure 5. Fit of column densities of carbon dioxide, carbon monoxide, and carboxylic acids produced during radiation exposure (0.1 μA, 1 μA) at 10 K. Two separate fits for pathway A (blue) and B (black) are derived for each profile to test the sensitivity of the fitting procedure.

(A color version of this figure is available in the online journal.)

5. ASTROPHYSICAL IMPLICATIONS

The present laboratory study simulated the abiotic formation of carboxylic acids (RCOOH) in interstellar (Gibb et al. 2004) and solar system (Kerridge 1999) model ices of carbon dioxide (CO₂)–hydrocarbon mix C_nH_{2n+2} ($n = 1-6$). The abundance ratio (~19:1) of CO₂:individual hydrocarbons in this study is indeed comparable to those ratios found in polar interstellar ices (Gibb et al. 2004)—CO₂:CH₄ in infrared sources AFGL 989 (~10:1), S140 IRS 1 (~12:1), NGC 7538 IRS 1 (~13:1), and NGC 7538 IRS 9 (~10:1). It was of particular motivation to constrain the formation condition that possibly links the past, undefined processing of Murchison meteorite leading to the richness and diversity of carboxylic acids found in recent extracts (Huang et al. 2005; Martins et al. 2006). It also hinted at an alternative route of carboxylic acid formation under carbon-dioxide-rich planetary surface environments such as in Mars and Saturn’s icy satellites of Hyperion, Lapetus, and Phoebe, where the evidence of radiolyzed carbon dioxide ice surfaced

out or still to come (Filacchione et al. 2010; Benner et al. 2000; Hintze et al. 2010).

The present model ices were radiolyzed at 10 K by energetic electrons up to doses of 17 ± 2 eV, or an average LET of $5.5 \text{ keV } \mu\text{m}^{-1}$, matching the energy transfer of 10–20 MeV cosmic-ray particles that penetrate the entire icy grain—MeV ions are known to create cascades of collision-induced suprathermal knock-on particles, secondary electrons with kinetic energies up to a few keV, as well as photons with a fluence of 10^3 photons $\text{cm}^{-2} \text{ s}^{-1}$ (Kaiser & Roessler 1997; Kaiser 2002; Ehrenfreund et al. 2001). Employing in situ infrared spectroscopy, the radiolysis-induced formation of RCOOH was monitored at 10 K by the signature absorption of carbonyl $\nu(\text{C}=\text{O})$ at 1720 cm^{-1} (Figure 2), the temporal profile of which was numerically fit using two independent kinetic schemes (Figures 4 and 5). The reaction (12) was utilized for constraining the upper limit of acid column density during radiation phase at 10 K, as well as during warm-up phases up to 300 K in extrapolation (Table 2). The production yield of carboxylic acids at 10 K was determined

as much as $(1.2 \pm 0.1) \times 10^{17}$ molecules cm^{-2} by the end of $1 \mu\text{A}$ irradiation, equivalent to a yield of 39% at 10 K (Table 2). Indeed, the present study was an amplified example laid on the previous kinetics studies of the methane-carbon dioxide and water-carbon dioxide systems (reactions (3–8)) with the reaction mechanisms as generalized as in reactions (reactions 9–11): as far as in situ infrared spectroscopy applies, any hydrocarbon ($\text{C}_n\text{H}_{2n+2}$) neighboring carbon dioxide (CO_2) could radiolyze via unimolecular decomposition to atomic hydrogen and a hydrocarbon radical; hydrogen could react with carbon dioxide to the *trans*-HOCO radical, which recombines in the matrix cage with the hydrocarbon radical for a carboxylic acid. The irradiated model ices at 10 K were subsequently heated up with a gradient of $0.5 \text{ K minute}^{-1}$ to 300 K. This process in turn simulates the protostellar switch-on phase, during which periods icy grains deem to warm-up in hot molecular cores and to diffusively induce the recombination of organic radicals on grain surfaces to the current level of chemical complexity as observed in the star-forming regions (Garrod & Herbst 2006; Garrod et al. 2008). It revealed in our dual detection schemes (Figures 2 and 3), however, that the carboxylic acids do not sublime up to 150 K under the UHV conditions, nor gain extra intensities exclusive of those diffusion-induced radical processes (Garrod & Herbst 2006; Garrod et al. 2008). Instead, the acid temporal column densities rather decreased marginally (Table 2). Only notable at 155 K was the presence of alcohol (ROH) functional groups possibly blended in the stronger absorptions of carboxylic acids (Table 1). The further heating allowed those solid acids to sublime under UHV conditions upward about 160 K. Nonetheless, the acid residue still remained to be seen on the substrate within the detection limit at room temperature—about 10% the abundance level at 10 K. Many interstellar molecules, including carboxylic acids (RCOOH), are known to have their origins in interstellar icy grains and to survive the succeeding gravitational collapse to the star formation, just as evidenced in astronomical observations or in extracts of carbonaceous meteorites as simulated in the laboratory (Bernstein et al. 2002) including the present study. The detailed residue analysis will further warranty to determine the structural diversity of the acid residue, a potential to matching the level of richness found in Murchison (Huang et al. 2005; Martins et al. 2006).

This work was supported by the National Aeronautics Space Administration (NASA) Astrobiology Institute under Cooperative Agreement No. NNA09DA77 A issued through the Office of Space Science. Special thanks to Dr. C. Ennis (University of Hawaii) for comments on this manuscript.

REFERENCES

- Benner, S., Devine, K., Matveeva, L. N., & Powell, D. H. 2000, *Proc. Natl Acad. Sci.*, **97**, 2425
- Bennett, C. J., Chen, S.-H., Sun, B.-J., Chang, A. H. H., & Kaiser, R. I. 2007, *ApJ*, **660**, 1588
- Bennett, C. J., Jamieson, C., Mebel, A. M., & Kaiser, R. I. 2004, *Phys. Chem. Chem. Phys.*, **6**, 735
- Bennett, C. J., Jamieson, C. S., Osamura, Y., & Kaiser, R. I. 2006, *ApJ*, **653**, 792
- Bennett, C. J., & Kaiser, R. I. 2007, *ApJ*, **660**, 1289
- Bernstein, M. P., Ashbourn, S. F., Sandford, S. A., & Allamandola, L. J. 2004, *ApJ*, **601**, 365
- Bernstein, M. P., Dworkin, J. P., Sandford, S. A., Cooper, G. W., & Allamandola, L. J. 2002, *Nature*, **416**, 401
- Bohn, R. B., Sandford, S. A., Allamandola, L. J., & Cruikshank, D. P. 1994, *Icarus*, **111**, 151
- Botta, O., & Bada, J. L. 2002, *Surv. Geophys.*, **23**, 411
- Cazaux, S., Tielens, A. G. G. M., Ceccarelli, C., Casets, A., Wakelam, V., Caux, E., Parise, B., & Teyssier, D. 2003, *ApJ*, **593**, L51
- Cronin, J. R., & Chang, S. 1993, in the Chemistry of Life's Origins, ed. J. M. Greenberg et al. (Dordrecht: Kluwer), 209
- Dartnell, L. R., Desorgher, L., Ward, J. M., & Coates, A. J. 2007, *Geophys. Res. Lett.*, **34**, L02207
- DelloRusso, N., Khanna, R. K., & Moore, M. H. 1993, *J. Geophys. Res.*, **98**, 5505
- Donnay, J. D. H., & Ondik, H. M. 1972, Crystal Data Determination Tables, Vol. 1 (3rd ed.; Washington, DC: NBS)
- Drouin, D., Couture, A. R., Gauvin, R., Hovington, P., Horny, P., & Demers, H. 2001, Monte Carlo Simulation of Electron Trajectory in Solids (CASINO ver. 2.42; Sherbrooke: Univ. Sherbrooke)
- Ehrenfreund, P., Bernstein, M. P., Dworkin, J. P., Sandford, S. A., & Allamandola, L. J. 2001, *ApJ*, **550**, L95
- Ehrenfreund, P., & Charnley, S. B. 2000, *ARA&A*, **38**, 427
- Filacchione, G., et al. 2010, *Icarus*, **206**, 507
- Frenklach, M., Packard, A., & Feeley, R. 2007, in Modeling of Chemical Reactions, ed. R. W. Carr (Elsevier Series Comprehensive Chemical Kinetics, Vol. 42; Amsterdam: Elsevier), 243
- Frenklach, M., Wang, H., & Rabinowitz, M. J. 1992, *Prog. Energy Combust. Sci.*, **18**, 47
- Garrod, R. T., & Herbst, E. 2006, *A&A*, **457**, 927
- Garrod, R. T., Weaver, S. L. W., & Herbst, E. 2008, *ApJ*, **682**, 283
- Gibb, E. L., Whittet, D. C. B., Boogert, A. C. A., & Tielens, A. G. G. M. 2004, *ApJS*, **151**, 35
- Hintze, P. E., Buhler, C. R., Schuerger, A. C., Calle, L. M., & Calle, C. I. 2010, *Icarus*, **208**, 749
- Hollis, J. M., Vogel, S. N., Snyder, L. E., Jewell, P. R., & Lovas, F. J. 2001, *ApJ*, **554**, L81
- Huang, Y., Wang, Y., Alexandre, M. R., Lee, T., Rose-Petrucci, C., Fuller, M., & Pizzarello, S. 2005, *Geochim. Cosmochim. Acta*, **69**, 1073
- Irlé, S., & Morokuma, K. 2000, *J. Chem. Phys.*, **113**, 6139
- Jamieson, C., Mebel, A. M., & Kaiser, R. I. 2006, *ApJS*, **163**, 184
- Kaiser, R. I. 2002, *Chem. Rev.*, **102**, 1309
- Kaiser, R. I., Eich, G., Gabrysch, A., & Roessler, K. 1999, *A&A*, **346**, 340
- Kaiser, R. I., Gabrysch, A., & Roessler, K. 1995a, *Rev. Sci. Instrum.*, **66**, 3058
- Kaiser, R. I., Jansen, P., Peterson, K., & Roessler, K. 1995b, *Rev. Sci. Instrum.*, **66**, 5226
- Kaiser, R. I., & Roessler, K. 1997, *ApJ*, **475**, 144
- Kerridge, J. F. 1999, *Space Sci. Rev.*, **90**, 275
- Kim, Y. S., Bennett, C. J., Chen, L.-H., O'Brian, K., & Kaiser, R. I. 2010, *ApJ*, **711**, 744
- Lattalais, M., Pauzat, F., Ellinger, Y., & Ceccarelli, C. 2009, *ApJ*, **696**, L133
- Martins, Z., Watson, J. S., Sephton, M. A., Botta, O., Ehrenfreund, P., & Gilmour, I. 2006, *Meteorit. Planet. Sci.*, **41**, 1073
- McDonald, G. D., Whited, L. J., DeRuiter, C., Khare, B. N., Patnaik, A., & Sagan, C. 1996, *Icarus*, **122**, 107
- Mehring, D. M., Snyder, L. E., Miao, Y., & Lovas, F. J. 1997, *ApJ*, **480**, L71
- Moore, M. H., & Hudson, R. L. 2003, *Icarus*, **161**, 486
- Muñoz Caro, G. M., & Schutte, W. A. 2003, *A&A*, **412**, 121
- Pizzarello, S. 2007, *Orig. Life. Evol. Biosph.*, **37**, 341
- Puletti, F., Mallocci, G., Mulas, G., & Cecchi-Pestellini, C. 2010, *MNRAS*, **402**, 1667
- Refson, K., & Pawley, G. S. 1986, *Acta Crystallogr. B*, **42**, 402
- Remijan, A., Snyder, L. E., Friedel, D. N., Liu, S.-Y., & Shah, R. Y. 2003, *ApJ*, **590**, 314
- Remijan, A., Snyder, L. E., Liu, S.-Y., Mehring, D., & Kuan, Y.-J. 2002, *ApJ*, **576**, 264
- Sander, W., & Gantenberg, M. 2005, *Spectrochim. Acta A*, **62**, 902
- Schidrowski, M. 1993, in the Chemistry of Life's Origins, ed. J. M. Greenberg et al. (Dordrecht: Kluwer), 389
- Shiao, Y.-S. J., Looney, L. W., Remijan, A., Snyder, L. E., & Friedel, D. N. 2010, *ApJ*, **716**, 286
- Socrates, G. 2001, Infrared and Raman Characteristic Group Frequencies (3rd ed.; New York: Wiley)
- Stalport, F., Coll, P., Szopa, C., Cottin, H., & Raulin, F. 2009, *Astrobiology*, **9**, 543
- Yuen, G. U., & Kvenvolden, K. A. 1973, *Nature*, **246**, 301
- Zheng, W., Jewitt, D., & Kaiser, R. I. 2006, *ApJ*, **639**, 534
- Zheng, W., Jewitt, D., Osamura, Y., & Kaiser, R. I. 2008, *ApJ*, **674**, 1242
- Zheng, W., & Kaiser, R. I. 2007, *Chem. Phys. Lett.*, **450**, 55